J Mater Sci (2008) 43:2026–2034
DOI 10.1007/s10853-007-2422-z

Quantitative fractography for estimating whole bone properties of manatee rib bones

Kari B. Clifton · Roger L. Reep · John J. Mecholsky Jr.

Received: 3 April 2007 / Accepted: 19 December 2007 / Published online: 31 January 2008

Abstract The goals of this study were to estimate the stress at failure and the fracture toughness of whole manatee ribs fractured in impact; and to determine whether typical watercraft are capable of generating enough energy to break manatee ribs upon impact. The unique construction of manatee ribs enabled us to apply quantitative fractographic techniques to measure some fracture mechanics parameters. Adult manatee bone behaves more like a ceramic than other types of bone. Due to this, we were able to see many of the features observed for brittle fracture in ceramics. We were able to identify crack origins, and make quantitative measurements of crack size. Failure stress was constant across body size despite the increase in rib size as the animals grow. Similarly, flaw size was the same for all animals regardless of body size. Fracture toughness for whole ribs (measured as the critical stress intensity factor, K_C) calculated from strain gage data was 8 MPa $m^{1/2}$. This value was greater than that reported for small sample specimens, suggestive of R-curve behavior in this bone. There were no differences between the sexes in their ability to resist fracture. Kinetic energy calculations indicated that recreational boats commonly found in Florida waters are capable of generating sufficient energy to fracture manatee ribs upon impact.

K. B. Clifton · R. L. Reep
Physiological Sciences, University of Florida, 1600 SW Archer Rd., Box 100144 HSC, Gainesville, FL 32610, USA

K. B. Clifton (✉)
Endocrine Research Unit, Jo-194, Mayo Clinic College of Medicine, 200 First St. SW, Rochester, MN 55905, USA
e-mail: clifton.kari@mayo.edu

J. J. Mecholsky Jr.
Materials Science and Engineering, University of Florida, P.O. Box 116400, Gainesville, FL 32611, USA

Introduction

The endangered Florida manatee shares its nearshore, coastal habitat with an ever increasing number of boats. Each year, 25–30% of all manatee deaths are a result of collisions with watercraft. Unlike other mammals, their rib cage is dorsal, running the entire length of the back. Broken ribs resulting from boat strikes cause severe damage to the lungs and other underlying soft tissues, frequently resulting in death. Boat speed zones are the primary tool for ameliorating the lethal interactions. However, existing speed limits are not based explicitly on information pertaining to the nature or severity of the injury, including bone fractures. In an effort to establish safer boat speeds for manatees, the Florida manatee recovery plan calls for research on the mechanical characteristics of manatee bone to better understand the effects of watercraft-related impacts [1]. This study is the first to estimate mechanical properties of whole manatee bone.

Quantitative fractography is a technique that uses principles of fracture mechanics to analyze fracture surfaces of materials such as ceramics [2, 3]. The strength of a brittle material is determined by the size of the fracture initiating crack, or flaw, and the fracture toughness of the material. Location of the crack can often be determined by examining the markings on the fracture surface.

Two features of manatee bone allowed us to use quantitative fractography to measure its mechanical parameters. First, all the ribs and other long bones are constructed of solid cortical bone; there are no marrow cavities or spongy bone. This feature, unusual for mammalian bone, is thought to be an adaptation to aid in hydrostasis [4]. Second, manatee bone often undergoes brittle fracture in static tests [5, 6]. Bone typically behaves as a quasi-brittle solid [7]. However, fully

mineralized bone from adult manatees does not undergo any post-yield plastic deformation [5].

The first goal of this study was to estimate the stress at failure and the fracture toughness of whole manatee ribs fractured in impact. Fracture toughness is the ability to resist fracture, one measure of which is the critical stress intensity factor (K_C). This is an estimate of the amount of energy required to propagate a macrocrack that leads to fracture [8]. Toughness is an important property because a tough bone is resistant to fracture, and this is most important when bone is impacted [9, 10]. Since adult manatee bone fails in a brittle manner when loaded statically at stressing rates $>$ 1 MPa/s, based on preliminary tests, it is assumed for this study that fracture resistance measured by K_C is similar to a measure of toughness in manatee bone loaded in impact. The second goal of this study was to address the hypothesis that forces generated by recreational watercraft under normal operation are sufficient to inflict skeletal injuries to manatees. We compared the estimated energy needed to fracture manatee ribs, both with and without overlying soft tissues, to that generated by common recreational watercraft operating in Florida waters.

Materials and methods

Bone sample collection

Ribs from 20 animals of both sexes, in three age classes (i.e., calf, subadult, and adult) were obtained from the Florida Fish and Wildlife Conservation Commission's Marine Mammal Pathobiology Laboratory. Collection and use of tissues for research was conducted under U.S. Fish and Wildlife Service permit #MA067116-0 issued to the University of Florida. By convention, total body length was used as a proxy for age, and individuals were assigned to age classes based on established size definitions [11]. Bones were obtained from fresh carcasses at the time of necropsy. One rib from the mid-thoracic region of each animal was collected and stored at −20 °C until testing. Bones were cleaned of soft tissues and tested wet, at room temperature.

Whole rib impact testing

Whole ribs were impacted using a compressed air gun at the Structures Laboratory in the Department of Coastal and Civil Engineering at the University of Florida (Fig. 1). The barrel is 6 m in length with a 10 cm inner diameter. The gun is equipped with a compressor that allows projectiles to be fired at a range of speeds, and two photocells and an oscilloscope to record the speed of the projectile as it exits the barrel. Ribs were positioned vertically in a fixture that was mounted on a steel frame, so that the lateral (convex) side of the rib faced the gun, and the concave side faced the frame. They were impacted perpendicular to their long axis, in the middle of the lateral side with a 5 cm × 10 cm × 1.2 m pine projectile. The leading end of the projectile was equipped with a hemispherical nosepiece coated in fiberglass. The mass of the projectile was 13 kg. The distance between the end of the barrel and the rib was 2.3 m. The projectile was fired between 23 and 28 m/s.

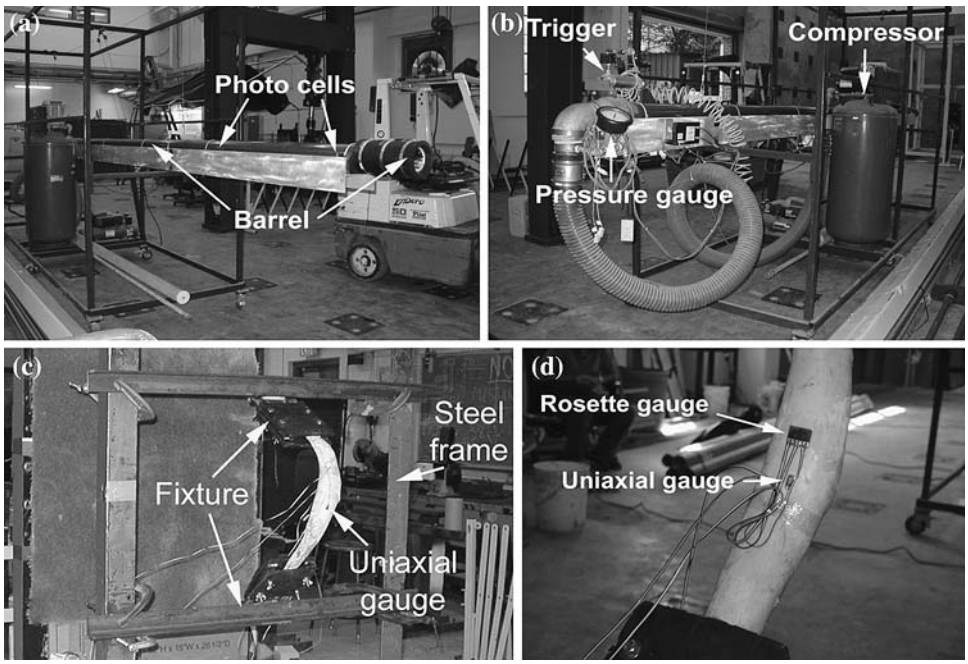

Fig. 1 Setup for impact tests of whole manatee ribs. (**a**) Compressed air gun assembly. The barrel is a 20′ PVC pipe with a 4″ diameter. The end of the barrel is equipped with two photocells to measure the velocity of the projectile. (**b**) The gun is equipped with a compressor, pressure gage, and trigger. (**c**) Manatee rib positioned in test fixture, mounted on frame for impact testing. The rib is outfitted with a uniaxial strain gage on the convex (lateral) surface. (**d**) View of the concave (pleural, or medial) side. This side is outfitted with a uniaxial and a rosette strain gage. The intended area of impact is between these two gages

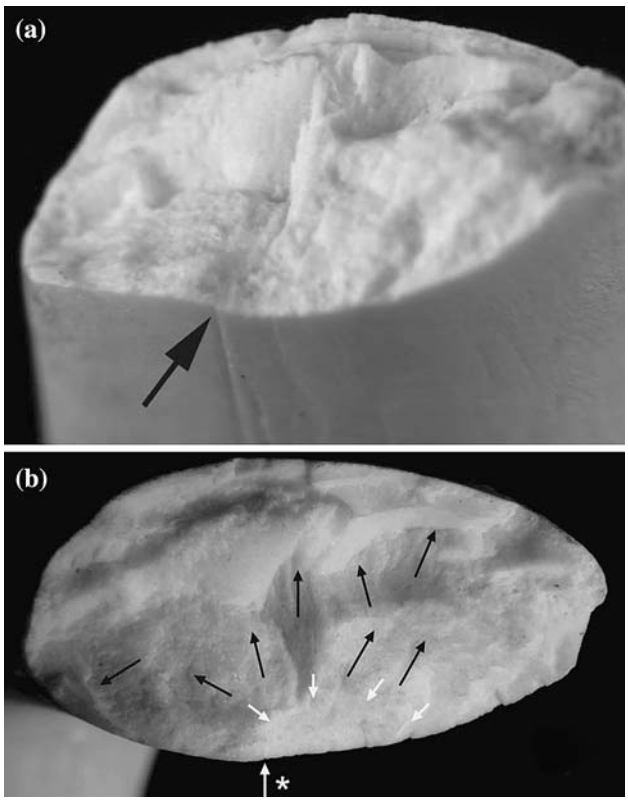

Fig. 2 Two views of a fracture surface of a manatee rib. (**a**) Examination of fracture surface indicated that the crack that led to failure originated at a groove on the medial surface (arrow). (**b**) White arrows indicate the extent of the fracture-initiating crack. * marks the location of the natural groove shown in Fig. 2(**a**). Black arrows show the direction of crack propagation as indicated by the hackle markings

Quantitative fractography was used to identify the fracture origin and measure crack size for each rib (Fig. 2a). The failure stress (σ) was calculated as

$$\sigma = \frac{K_C}{Y(c)^{1/2}} \tag{1}$$

where K_C is fracture toughness (MPa $m^{1/2}$), measured as the critical stress intensity factor, Y is a geometric factor based on crack shape and loading conditions, and c is the crack size (m) [3]. Y is assumed to be 1.25 based on the fact that the cracks were approximately semi-elliptical and their magnitudes were $\sim$1/10 of the depth of the rib cross-sections; thus, these crack sizes can be considered small relative to the depth [12]. Values for K_C were taken from the middle region of the adjacent rib, which were calculated in a study of the material properties of manatee bone [5]. The value used was the mean for the mid section of the adjacent rib. Crack size (c) was calculated as

$$c = (a \cdot b)^{1/2} \tag{2}$$

where a and b are crack depth and half-width (in meters), respectively, as measured from the fracture surface with digital calipers to the nearest 0.1 mm. The assumption in Eq. (2) provides the Y factor for the equivalent semi-circular crack. This has been shown to be equivalent for $a/b > 0.1$ to the more conventional method of calculating the elliptical integral of the second kind with the actual elliptical dimensions [13, 14].

Strain gage testing

To validate the failure stress calculations, three additional ribs were outfitted with strain gages to directly measure strain during impact (Fig. 1d). For each rib, a uniaxial gage (CEA-06-250UN-350, Vishay Micro-Measurements, Raleigh, NC) was placed on the lateral (convex) surface, and a uniaxial gage and a rosette gage (CEA-06-125UR-350) were placed on the pleural (concave) side. Gages were placed along the midline, parallel to the long axis, either just above or below the center of the rib. The center element of the rosette was oriented parallel to the long axis of the bone. Signals were output to an eight channel signal conditioner and sampled at 50 kHz. Raw data were converted to microstrain, which were used to calculate the principal strains using standard formulae. Failure stress was calculated as

$$\sigma = E\varepsilon \tag{3}$$

where E is Young's modulus (GPa) measured with ultrasound (Nuson, Inc., Boalsburg, PA), and ε is the maximum principal strain.

As a check of the strain data, an additional rib was outfitted with gages and loaded to failure in quasi-static 3 point bending at a loading rate of 4.4 N/s. The signal was sampled at 20 Hz. Failure stress was calculated using the standard formula for a curved beam in bending. For all gaged ribs, the fracture origin was identified fractographically, and fracture toughness (K_C) was determined using measured values of c and σ (Eq. 1). Fracture toughness values calculated for whole ribs were compared to those from the material test specimens [5] to assess the validity of using the materials values in the failure stress calculations. Cross-sectional area of the ribs at the fracture site was calculated to the nearest mm^2 (Table 1).

Kinetic energy calculations

The most common recreational watercraft in operation in Florida waters is a 17′ vessel [15], which is typically equipped with a single outboard engine of 100–115 HP. A typical 17′ vessel at idle speed (i.e., no wake) is traveling at 2–3 mph (0.9–1.3 m/s) depending on vessel configuration, and 10–12 mph (4.5–5.4 m/s) corresponds to a boat

Table 1 Mechanical property and fractography data for 22 manatee ribs fractured in impact

Animal	Sex	TL (cm)	Age	Rib area (mm^2)	c (m)	K_C (MPa $m^{1/2}$)	σ_m (MPa)	σ_w (MPa)
MSTM0109	M	166	C	340	1.9E-03	2.5	46	142
MNW0207	F	188	S	413	1.9E-03	2.4	45	145
MSW0227	F	190	S	512	2.5E-03	2.3	37	125
MSTM0113	M	196	S	456	1.5E-03	2.0	41	159
MSW0057	M	201	S	450	1.5E-03	2.2	46	163
MSE0205	M	238	S	732	1.8E-03	2.5	48	149
MSW0160	F	246	S	778	1.8E-03	2.7	52	148
MSTM0102	F	265	S	1,207	1.5E-03	2.5	51	159
MSW0165	F	267	S	1,060	2.7E-03	2.5	45	120
MSW0251	M	276	A	959	2.4E-03	3.0	50	128
MSW0225	F	282	A	1,518	2.4E-03	3.0	49	127
MSW0223	F	294	A	1,413	2.2E-03	2.7	46	133
MSW0208	F	299	A	1,360	2.7E-03	2.8	43	120
MEC0213	F	314	A	1,134	1.5E-03	2.7	61	176
MSW0226	M	315	A	1,021	2.8E-03	2.7	41	118
MSW0239	M	321	A	1,890	1.6E-03	2.5	56	175
MSW0253	M	327	A	1,887	2.3E-03	2.7	46	130
MSTM0414	F	335	A	1,926	2.0E-03	2.8	50	138
MNW0208#6	M	343	A	1,346	2.3E-03	2.9	48	129
MNW0208#9	M	343	A	–	1.5E-03	2.9	67	179
MNW0208#10	M	343	A	1,204	3.5E-03	2.9	40	106
MSW0245	M	344	A	2,039	2.2E-03	2.4	41	133

Variables are: animal, code represents region, year, and carcass number; sex: male (M) or female (F); total body length (TL); age classes: calf (C), subadult (S), or adult (A); rib area; crack size (c); fracture toughness from small specimens (K_C); and failure stresses (σ_m calculated with fracture toughness data from machined, small specimen tests [Eq. (1)], and σ_w calculated from estimated whole bone fracture toughness [Eq. (1)]). Rib area is cross-sectional area at fracture site. Three ribs were tested for animal MNW0208 (rib number indicated). –indicates no data for that rib

traveling at or near hull speed (i.e., on a plane). Maximum speed is approximately 35–40 mph (15.6–17.9 m/s). Weights for a few common 17′ vessels with the recommended engines were taken from the specifications posted on manufacturers' websites. Kinetic energy (KE) was calculated for speeds of 2, 10, and 35 mph (0.9, 4.5, and 15.6 m/s, respectively) as

$$\mathrm{KE} = 1/2mv^2 \quad (4)$$

where m is the mass of the projectile (kg), and v is velocity (m/s). We assumed one adult operator (200 lbs.) and one half-tank of fuel. The KE of the projectile was calculated using the mass and velocity given above. The soft tissues overlying bone have been shown to absorb and dissipate impact energy, thereby decreasing the energy transferred to the skeleton [16–18]. To estimate the energy-damping ability of the tissues overlying the ribs, soft tissue thickness (e.g., skin, blubber, muscle) was measured approximately one-third of the way down from the head of the ribs on some whole body sections. Robinovitch et al. [18] measured the amount of impact energy transferred to the femoral trochanter with overlying soft tissues of varying thickness. Tissue energy absorption was regressed against soft tissue thickness to determine the threshold of tissue thickness needed to prevent femur fracture during falls in the elderly. We used their regression to estimate the amount of energy dissipated by manatee soft tissues. Kinetic energy curves for the boats were graphically compared to the kinetic energy of the projectile used to impact the bare rib, as well as to the estimate for ribs with overlying soft tissues.

Statistical analyses

Failure stress was compared between sexes and age classes in separate one-way ANOVAs [19]. Failure stress and crack size were regressed against total body length, and failure stress was regressed against rib cross-sectional area. Analyses were performed with SAS v. 9.1 [20].

Results

Whole rib impact tests

Mechanical property and fractographic data from the impact tests are presented in Table 1. A total of 23 ribs from 20 animals were used in this study; 22 ribs were fractured in impact, and one was tested in quasi-static 3 point bending. Only one calf was tested, as the small size of the ribs made them difficult to test. The lone calf was omitted from the analysis by age class. Of the other 19

Table 2 Mean mechanical data by sex and age class

Group	σ_m (MPa)	σ_w (MPa)
Sex (ages pooled)		
Females (10)	48 ± 6	139 ± 18
Males (12)	46 ± 8	143 ± 23
Age class (sexes pooled)		
Subadults (8)	48 ± 5	146 ± 16
Adults (13)	49 ± 8	137 ± 24

Variables are failure stress (σ_m) and adjusted failure stress (σ_w). Values are mean ± SD. Sample sizes are reported in parentheses for each group. No groups were significantly different ($p > 0.05$)

animals, eight were subadults (i.e., juveniles) and 11 were adults. The sexes were represented equally, ten females and ten males. Mean failure stress was calculated, using Eq. (1) and data from Table 1, to be 47 ± 7 MPa, varying from 37 to 67 MPa. Mean adjusted failure stress (see below) was 139 ± 21 MPa (range 106–179 MPa). Means by sex and age class are reported in Table 2. There were no statistically significant differences between failure stress by sex (ANOVA, $p = 0.51$) or by age class ($p = 0.19$). The regressions of crack size against total body length ($p = 0.16$, Fig. 3) and of failure stress against total body length ($p = 0.55$) indicated no relationship of either variable to body size. Similarly, there was no relationship between rib cross-sectional area and failure stress ($p = 0.54$, Fig. 4). This implies that the ability to resist bone fracture in impact does not increase as animals grow.

Strain gage tests

Of the 22 ribs impacted, three were outfitted with strain gages. However, data were successfully collected for only

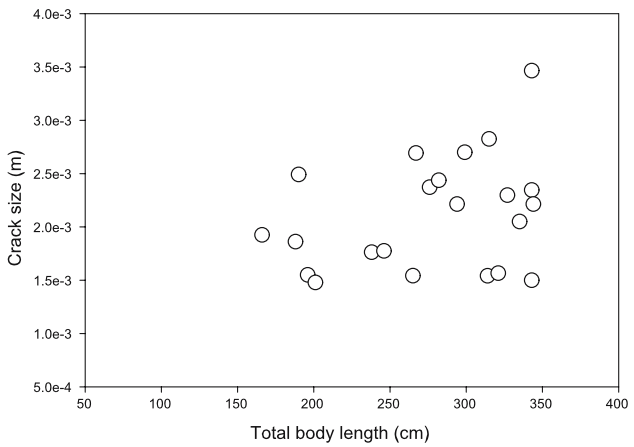

Fig. 3 Whole rib crack size versus total body length. There was no relationship between flaw size and total body length ($R^2 = 0.09$, $p = 0.16$). Flaw size is the same regardless of rib cross-sectional area, which increases with total body size

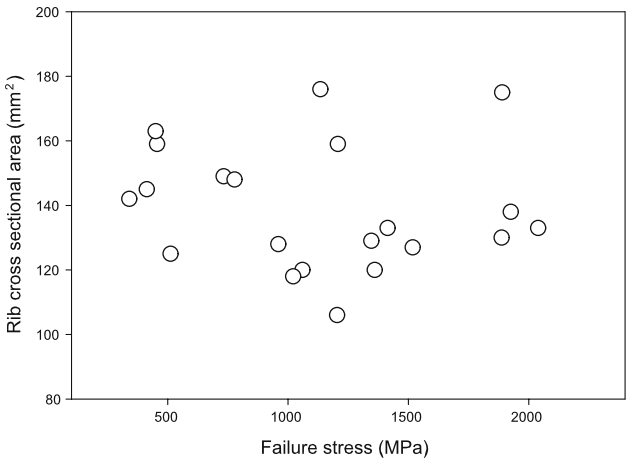

Fig. 4 Rib cross-sectional area versus failure stress. There was no relationship between cross-sectional area and failure stress ($R^2 = 0.02$, $p = 0.54$)

one (MNW0208 #6, Table 3). The lone rib tested in quasi-static 3 point bending (MNW0208 #14, Table 3) was also outfitted with gages; it failed at a load of 4744 N. Peak strains and failure stresses for the impact and quasi-static tests were very similar (0.56% and 0.61%, respectively). Fracture toughness calculated for the impacted rib was 7.7 MPa $m^{1/2}$, essentially identical to the 7.8 MPa $m^{1/2}$ for the rib from the quasi-static test. These values were much greater than those used for the failure stress calculations reported in Table 1. Our results indicate that it is not appropriate to use the small specimen fracture toughness values to calculate whole bone failure stress. By doing so, stresses were most likely underestimated. To adjust for this, 8 MPa $m^{1/2}$ was used to derive more appropriate estimates of failure stress using Eq. (1), reported as σ_w in Table 1.

In order to help further explain the high toughness values we obtained for the whole ribs, we calculated the expected strength of the rib tested in quasi-static 3 point bending using curved beam theory with an approximately elliptical cross-section [21]. A failure stress of 210 MPa

Table 3 Mechanical and fractographic data for strain gaged ribs

Rib #	Peak microstrain	Modulus (GPa)	Failure stress (MPa)	Crack size (m)	Toughness (MPa $m^{1/2}$)
6	6,075	21	128	2.3E-03	7.7
14	5,577	19	106	3.5E-03	7.8
14[a]	5,577	35	194		

Ribs from animal MNW0208. Rib #6 was tested in impact, rib #14 in quasi-static 3 point bending. Young's modulus was measured with ultrasound. Failure stress was calculated as $\sigma = E\varepsilon$. Crack size, c (m), as measured from the fracture surface. Fracture toughness calculated from Eq. (1)

[a] Modulus and failure stress calculated from stress–strain curve

was calculated for the rib MNW0208 #14 using the failure load of 4744N. At best, this is a very rough estimate because of the extremely complicated shape of the bone. This value is greater than the 106 MPa calculated from the microstrain and ultrasound modulus for this rib (Table 3). However, the elastic modulus calculated from the stress–strain curve generated from the quasi-static test was 35 GPa, which translates to a failure stress of 194 MPa (Table 3), in close agreement with the curved beam calculation. These calculated failure stresses are quite reasonable compared to stresses determined fractographically in Table 1. Coincidently, both the high and low values (106 and 179 MPa) are for this same animal, MNW0208.

Kinetic energy calculations

Projectile velocity, as measured exiting the barrel, was 23–28 m/s. To make conservative estimates of the threshold for fracture we used the maximum projectile velocity (28 m/s) for calculations. Vessel configurations and kinetic energies are presented in Tables 4 and 5, and Fig. 5. Based on the configurations selected, rib fracture can occur at speeds of 7–8 mph, or just below hull speed. This is the estimated speed at which boats generated kinetic energy equal to that of the projectile, as determined by the point at which the regression curves cross the kinetic energy line for the projectile. This estimate is for bare bone, which of course is not a realistic scenario. The maximum thickness of manatee soft tissues overlying the ribs was 58 mm. Robinovitch et al. [18] measured impact energy absorption for soft tissues up to 43 mm thickness. Using their regression, we extrapolated the amount of energy dissipated by the manatee soft tissues to be 70%. That is, only 30% of impact energy is transferred to the bone. This projection is plotted on Fig. 5, as the "with skin" plot. At this energy absorption estimate, boat speeds of 13–15 miles per hour are sufficient to fracture manatee ribs (i.e., where the regression curves cross the "with skin" kinetic energy estimate, indicated by the vertical lines).

Table 5 Kinetic energy calculations for vessel configurations and impact projectile

Manatee	Kinetic energy (kJ)	Boat	Kinetic energy (kJ)		
			2 mph	10 mph	35 mph
Bare bone	5	Maverick	0.40	10	121
With skin	17	Mako	0.35	9	106
		Key West	0.30	8	93

Energy for bare bone is the kinetic energy of the projectile. With skin is the minimum amount of kinetic energy needed to create a fracture based on the calculated 70% energy absorption by manatee soft tissues

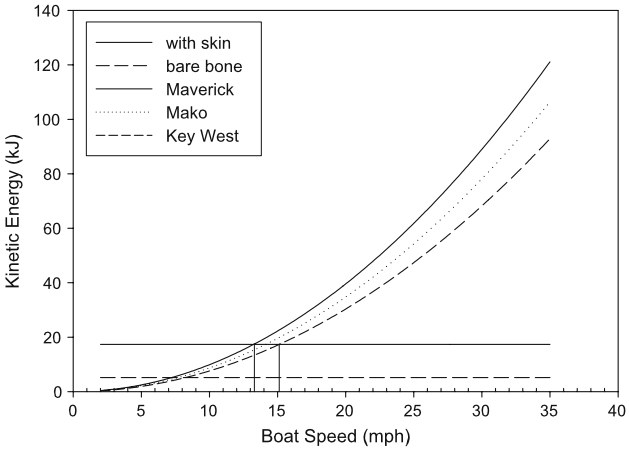

Fig. 5 Kinetic energy as a function of boat speed. Three vessel configurations are presented. Calculated kinetic energy of the projectile impacting bare bone is plotted, along with an energy estimate with overlying soft tissues in place (with skin). With an estimated 70% of the total kinetic energy being dissipated by the soft tissues, minimum boat speeds capable of producing rib fracture are ~13–15 mph (vertical lines)

Table 4 Boat data for kinetic energy calculations

Boat	Boat length	Boat weight (kg)	Fuel tank (gal)	Fuel weight (kg)	Engine (HP)	Engine weight (kg)	Boater weight (kg)	Total weight (kg)
Maverick[a]	17′0″	684	40	53	115	162	91	989
Mako[b]	17′3″	567	37	49	115	162	91	869
Key West[c]	17′6″	454	40	53	100	161	91	758

Boat weights were taken from manufacturers' specifications posted on their official websites. Fuel weight is for one half tank. Total weight is equal to the sum of weights for the vessel, fuel, engine, and one passenger

[a] Maverick Boat Company, Inc., 2004. Model: 17′ Master Angler

[b] Mako Marine International, Inc., 2005. Model: 171 Center Console

[c] Key West Boats, Inc., 2005. Model: 1760 Stealth

Discussion

Fracture toughness

There was no relationship between failure stress and total body length (a proxy for age) for the manatees in this study. Failure stress (Table 1) and critical crack sizes (Fig. 3) for the whole ribs were similar for all animals regardless of total body length; likewise, there was no correlation between cross-sectional area of ribs and failure stress (Fig. 4). Clifton et al. [5] reported that fracture toughness (reported as K_C), material density, and mineral content did not vary significantly over the range of body sizes. If these values accurately reflect the material properties of rib bone, then the finding of non-significant variation in critical crack size and failure stress in whole bones with rib size is not anomalous. Manatees have unique ribs that continue to grow in diameter even after longitudinal growth of the animal as ceased. We expected that this would result in an increase in strength and toughness for larger ribs over smaller ones. But despite the increase in rib size (340–2,039 mm^2 cross-sectional area) in manatees, there is no concomitant increase in ability to resist crack formation because the material is essentially the same.

R-curve behavior and viscoelasticity in bone

The greater fracture toughness values calculated from the strain data relative to the values measured from the small specimens of Clifton et al. [5] may be indicative of R-curve behavior in manatee bone. Those values, measured from machined specimens tested in 3 point bending, ranged from 2.0 to 3.0 MPa $m^{1/2}$, compared to 8 MPa $m^{1/2}$ for the whole ribs tested here. Another study [6] for specimens whose sample sizes were between the machined test specimens and the whole bones found a mean fracture toughness of 4.5 MPa $m^{1/2}$. This increase in toughness with increased specimen size, implying increased crack size, is suggestive of a material with a rising resistance curve, or R-curve. A rising R-curve describes an increase in fracture toughness with the increase in crack extension [22]. This behavior is characteristic of quasi-brittle materials such as some ceramics, and has now been documented in human, bovine, equine, and deer antler bone [23–26]. If manatee bone exhibits R-curve behavior, then it is not appropriate to use toughness values from small sample material properties tests to calculate failure stresses of whole bones. In addition, the value of strength obtained from the curved beam calculation is greater than the strain gage value, not a factor 3 times less than the estimates, as are the values obtained from the small rectangular beam specimens. The result of the calculation of the curved beam further supports the idea that R-curve behavior may be active in the fracture of manatee rib bones and that the greater strength values, calculated assuming a fracture toughness of 8 MPa $m^{1/2}$ with the measured crack sizes, are accurate.

True brittle materials exhibit flat R-curve behavior [7, 26]. The material tests of adult manatee bone show that machined specimens tested in static 3 point bending undergo very little or no plastic deformation; typically they fail catastrophically near the yield point [5]. This seemingly contradicts the toughness data presented here that suggests R-curve behavior. However, Vashishth et al. [26] point out that some ceramics do produce rising R-curves. Like all bone, manatee bone is a ceramic-polymer composite of complex, hierarchical structure. Bone microstructure, mineral density, and collagen content all affect the R-curve behavior [23–26]. Malik et al. [24] reported lower R-curves in bone of increased stiffness, tested in tension. Nalla et al. [25] reported an age-related decrease in both crack initiation and crack growth resistance. The high mineral content of manatee bone (mean 69%) likely has a similar effect. Additionally, bone microsctructural features may influence R-curve at different scales. For example, interlamellar spaces or blood vessel channels might influence fracture toughness of whole bones, but distribution of osteons would only affect toughness in smaller, machined specimens. Finally, the complex shape of these ribs makes it difficult to determine the accuracy of our stress calculations; other techniques such as finite element analysis may provide better estimates. Appropriate testing needs to be done to characterize R-curve behavior in manatee bone.

The R-curve behavior of manatee bone is likely due to the effect of crack size on the local microstructure. A larger sample allows for a greater crack size, and more collagen is available to contribute to the toughening, resulting in a larger fracture toughness, a feature generally attributable to viscoelasticity in bone. However, in the manatee ribs this effect is relatively small because the bone is highly mineralized [5], implying that, unlike other bone, manatee rib bone behaves much more as a ceramic than a ceramic-polymer composite. The difference in crack size between the small samples and the whole ribs simply reflects that there is much more collagen in the whole ribs. Therefore, absolute size most likely explains the greater fracture toughness of the whole ribs over the machined specimens. For some materials, including most bone, fracture toughness is dependent on strain rate. As strain rate increases, so does strength, modulus, and K_C [7]. However, note that work of fracture can decrease or remain the same with increased strain rate, also due to the viscoelastic nature of bone [12]. The different behavior of K_C versus work of fracture with strain rate is due to the method of

measurement of both. As the whole bones and the small sample specimens were tested at different rates, the effects of strain rate and specimen size are confounded. However, for all the small specimens, the stressing rates were >7 MPa/s [5]; this rate is considered fast enough to avoid possible viscoelastic effects.

Impact energy absorption of bone and soft tissues

Impact testing of human bone is often done to determine the loads at which bones such as the femur break. The whole manatee rib tested in static 3 point bending failed at a load of 4,480 N, which is only moderately greater than the critical trochanteric impact load of 4,170 N, the average load required to fracture in impact the proximal femur in the elderly [17]. Soft tissues overlying the bone absorb impact energy, thereby reducing the load transferred to the bone. In femoral impact tests conducted by Robinovitch et al. [18] energy absorption varied from 6 to 58%. The authors found that for each millimeter increase of soft tissue thickness, peak load transferred to the bone decreased by 70 N, and soft tissue energy absorption increased by 1.7 J. In a different study [17], artificial hips protected by soft tissues were impacted at both high and low impact rates. Results showed that regardless of impact rate, 80% of the total load was transferred to the bone. In those two studies, impact energies of 132 J and 140 J were capable of creating fractures. Our projectile generated 5 kJ, so we likely could have created fractures in manatee ribs with much less force. Taking the soft tissues into consideration, our calculations indicated that a kinetic energy of 17 kJ is required to create rib fractures in manatees. Using the regression of Robinovitch et al. [18], 12 kJ of the 17 kJ (70%) would be dissipated by the soft tissues, and the remaining 5 kJ transferred to the skeleton; more than adequate to fracture manatee ribs. For the 17′ recreational vessels we selected, 17 kJ translates to speeds of 13–15 mph (Fig. 5).

We needed to make a few assumptions to generate this estimate. While the vessel weights are accurate, the total weight would likely be greater, as we did not include items such as the battery, safety equipment, other supplies or gear, or additional passengers. Greater vessel weights would shift the curves up, effectively lowering the vessel speed able to create fractures. More importantly, it may not be valid to use the energy/soft tissue thickness regression based on human tissues for manatees. The dermis of manatee skin is different from that of humans, and from that of other marine mammals [27], and likely has different energy-damping capabilities. To more accurately determine the position of the "with skin" line in Fig. 5, the compliance of manatee skin needs to be determined.

Summary

The goal of this study was 2-fold: to estimate the stress at failure and the fracture toughness of whole manatee ribs fractured in impact, and to determine if the typical watercraft found in Florida waters is able to generate enough force to break manatee ribs upon impact. The unique solid cortical bone construction of manatee ribs enabled us to apply fractographic techniques to measure some fracture mechanics parameters. Manatee bone behaves more like a ceramic than other types of bone. Due to this, we were able to see many of the features observed for brittle fracture in ceramics. We were able to identify crack origins, and make quantitative measurements of crack size. Failure stress was constant across body size, implying that the strength of ribs does not change as the animals grow, despite the increase in rib size. The impact tests performed here provide additional evidence that manatee bone behaves in a similar manner to brittle materials when loaded rapidly. For manatees, this means that the amount of impact energy needed to break ribs is not large, and our studies indicate that it does not change as the animals grow. Finally, we found that recreational boats typically found in Florida waters can easily generate enough impact force to break manatee ribs, leaving manatees highly susceptible to bone fracture from collision with boats.

Acknowledgements Funding was provided by a University of Florida College of Veterinary Medicine, The University of Florida University Scholars Program, the Florida Fish and Wildlife Conservation Commission, and the Sigma Xi Scientific Research Society. The Florida Fish and Wildlife Research Institute provided the bone samples. We gratefully acknowledge Chuck Broward for providing his expertise with the air cannon, and to Peter Ifju and Billy Schultz for the strain gage work and static testing. Thanks to Beth Carson, Travis Schrock, and Chris Woan for their assistance with this project. This research was conducted in accordance with IACUC guidelines at the University of Florida.

References

1. U.S. Fish, Wildlife Service (2000) In: Technical/Agency Draft, Florida Manatee recovery Plan, (*Trichechus manatus latirostris*), 3rd revision. U.S. Fish and Wildlife Service, Atlanta
2. Mecholsky JJ Jr (1993) In: Simmons CJ, El-Bayoumi OH (eds) Experimental techniques of glass science. American Ceramic Society, Westerville, p 483
3. Mecholsky JJ Jr (2001) In: Buchow KHJ (ed) Encyclopedia of materials: science and technology. Pergamon Press, Oxford, p 3257
4. Domning DP, de Buffrenil V (1991) Mar Mamm Sci 7:331
5. Clifton KB, Yan J, Mecholsky JJ Jr, Reep RL (2007) J Zool Lond. doi:10.1111/j.1469-7998.2007.00366.x
6. Yan J, Clifton KB, Reep RL, Mecholsky JJ Jr (2006) J Biomech 39:1066
7. Zioupos P (1998) Mater Sci Eng C 6:33

8. Mecholsky JJ Jr (1996) In: Varner JR, Frechette VD, Quinn GD (eds) Ceramic transations. Fractography of glasses and ceramics III. American Ceramic Society, Westerville, p 385
9. Wainwright SA, Biggs WD, Currey JD, Gosline JM (1982) In: Mechanical design in organisms. Princeton University Press, Princeton
10. Turner CH, Burr DB (1993) Bone 14:595
11. O'Shea TJ, Beck CA, Bonde RK, Kochman HI, Odell DK (1985) J Wildl Manage 49:1
12. Randall PN (1966) ASTM STP 410:88
13. Mecholsky JJ (1994) In: Bradt RC, Tressler RE (eds) Fractography of glass. Plenum Press, New York, p 43
14. Bansal GK (1976) J Am Ceram Soc 59:87
15. Wright SD, Ackerman BB, Bonde RK, Beck CA, Banowetz DJ (1995) In: O'Shea TJ, Ackerman BB, Percival HF (eds) Population biology of the Florida manatee. National Technical Information Service, Springfield, p 259
16. Nikolić V, Hančević J, Hudec M, Banović B (1975) Anat Embryol 148:215
17. Parkkari J, Kannus P, Heikkila J, Poutala J, Sievanen H, Vuori I (1995) J Bone Min Res 10:1437
18. Robinovitch SN, McMahon TA, Hayes WC (1995) J Orthop Res 13:956
19. Zar JH (1996) In: Biostatistical analysis. Prentice Hall, Upper Saddle River
20. SAS INSTITUTE INC. (1989) In: SAS/STAT user's guide, vol 2. SAS Institute Inc., Cary
21. Young WC (1989) In: Roark's formulas for stress and strain. McGraw-Hill, New York
22. Vashishth D (2004) J Biomech 37:943
23. Les CM, Stover SM, Keyak JH, Taylor KT, Kaneps AJ (2002) J Orthop Res 20:607
24. Malik CL, Stover SM, Martin RB, Gibeling JC (2003) J Biomech 36:191
25. Nalla RK, Kruzic JJ, Kinney JH, Ritchie RO (2004) Bone 35:1240
26. Vashishth D, Behiri JC, Bonfield W (1997) J Biomech 30:763
27. Kipps EK, McLellan WA, Rommel SA, Pabst DA (2002) Mar Mamm Sci 18:765